We are IntechOpen, the world's leading publisher of Open Access books Built by scientists, for scientists

4,800
Open access books available

122,000
International authors and editors

135M
Downloads

Our authors are among the

154
Countries delivered to

TOP 1%
most cited scientists

12.2%
Contributors from top 500 universities

CLARIVATE ANALYTICS BOOK CITATION INDEX INDEXED

WEB OF SCIENCE™

Selection of our books indexed in the Book Citation Index in Web of Science™ Core Collection (BKCI)

Interested in publishing with us?
Contact book.department@intechopen.com

Numbers displayed above are based on latest data collected.
For more information visit www.intechopen.com

14

Distinct Element Method Applied on Old Masonry Structures

Marwan Al-Heib
Ineris – Ecole des Mines de Nancy, Parc de Saurupt
France

1. Introduction

Masonry structures have specific aspects and different numerical approaches are available for studying their behavior. The analysis of masonry constructions is a complex task (Lourenco, 2002), especially under special loads and when the soil-structure interaction becomes essential for studying the real behavior. Usually, salient aspects are:

- Difficult and expensive characterization of the mechanical properties of the materials used;
- Large variability of mechanical properties, due to workmanship and use of natural materials;
- Significant changes in the core and constitution of structural elements, associated with long construction periods;
- Unknown construction sequence;
- Unknown existing damage in the structure.

In addition, under the different loading conditions, many experimental studies have shown that joints or interfaces are the weakest zones of masonry structures. Figure 1 shows some masonry failure modes, according to Sutcliffe et *al*., 2001.

Several methods and computational tools are available (Massart et al, 2005) for the assessment of the mechanical behavior of old constructions. The empirical approaches and the Eurocode (6) recommendations are generally satisfactory for engineers. The methods resort to different theories or approaches, resulting in: different levels of complexity (from simple graphical methods and hand calculations to complex mathematical formulations and large systems of non-linear equations), different availability for the practitioner (from readily available in any consulting engineer office to scarcely available in a few research-oriented institutions and large consulting offices), different time requirements (from a few seconds of computer time to a few days of processing) and, of course, different costs. Three approaches (Figure 2) are generally employed by engineers and researchers to model the masonry element: equivalent medium, discontinuous medium using continuous numerical approach (finite element and boundary element methods) and discontinuous medium using distinct element approach (distinct element method). The distinct element code will be employed herein to model masonry structures.

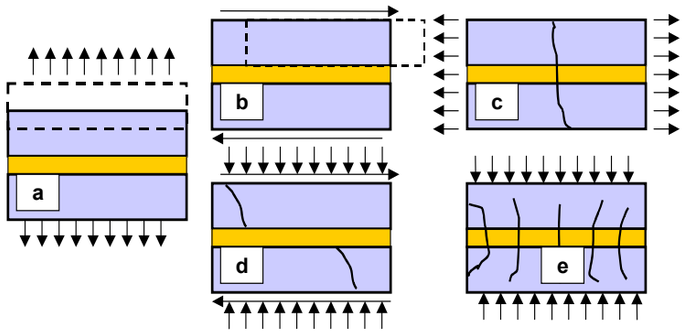

Fig. 1. Masonry failure modes a- direct tensile cracking of joint, b-sliding along joint c-cracking of unit and joint, diagonal tensile cracking of units e-compressive failure due to mortar militancy (Idris et al, 2009).

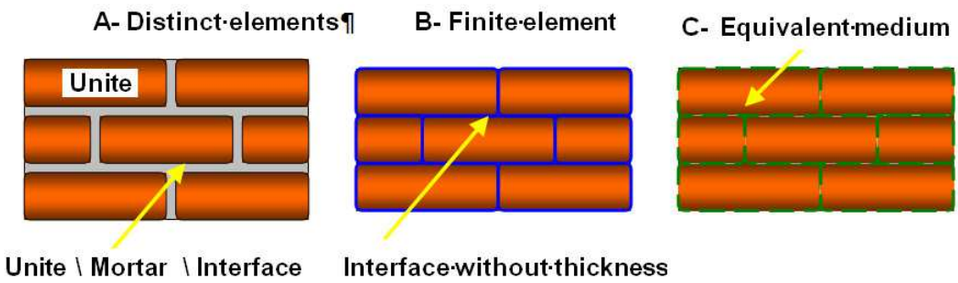

Fig. 2. Different approaches to model the behavior of masonry structures (Idris et al, 2009).

Two case studies will be presented in this chapter. The first case study concerns the simulation of the behavior of an underground structure of old tunnel supported by masonry of stone elements. The second case study concerns particularly the behavior of a masonry wall under the effect of an underground excavation (tunnel, mine, soil settlement, etc.).

2. Distinct element method

2.1 Description and background

A numerical model must represent two types of mechanical behavior in a discontinuous system: (1) behavior of the discontinuities; and (2) behavior of the solid material. In addition, the model must recognize the existence of contacts or interfaces between the discrete bodies that comprise the system. Numerical methods are divided into two groups according to the way in which they treat behavior in the normal direction of motion at contacts. In the first group (using a soft-contact approach), a finite normal stiffness is taken to represent the measurable stiffness that exists at a contact or joint.

The distinct element method was presented for the first time by Cundall in Nancy (1971), it considers the medium as an assembly of distinct rigid blocs that are linked together by joints. One can distinguish between rigid blocs and deformable blocs. Deformable blocs can be studied using the difference element method.

A discontinuous medium is distinguished from a continuous medium by the existence of interfaces or contacts between the discrete bodies that comprise the system. Discrete methods can be categorized both by the way they represent contacts and by the way they represent the discrete bodies in the numerical formulation.

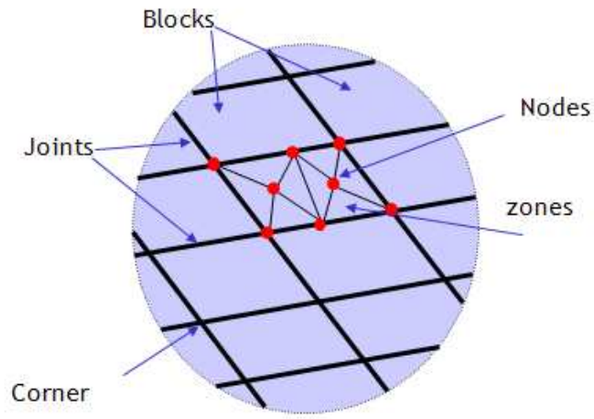

Fig. 3. Distinct element method and principal aspects.

In the second group (using a hard-contact approach), interpenetration is regarded as nonphysical, and algorithms are used to prevent any interpenetration of the two bodies that form a contact. The discrete (or distinct) element methods fall within the general classification of discontinuous analysis techniques. Originally used to model jointed and fractured rock masses (Tzamtzis et al, 2004), they were developed for the analysis of structures composed of particles or blocks and are especially suitable for problems in which a significant part of the deformation is accounted for by relative motion between blocks. *Masonry provides a natural application for these techniques*, as the deformation and failure modes of these structures are strongly dependent on the role of the joints. This approach is well suited for collapse analysis, and may thus provide support for studies of safety assessment, namely of historical stone masonry structures under earthquakes.

Two main features of the discrete element method (DEM) led to its use for the analysis of masonry structures. One is the allowance for large displacements and rotations between blocks, including their complete detachment. The other is the automatic detection of new contacts as the calculation progresses. Block material may be assumed rigid or deformable. Concerning masonry blocks, they are generally bonded by a lime or cement mortar. The model does not take the thickness of the mortar into account. Many numerical works have been performed for modeling masonry structures with the discrete elements methods (Verdel, 1994, Lemos, 1998). These studies looked essentially to the dynamic solicitation on dams and historic buildings.

2.2 Masonry joint modeling

In discrete element models, the representation of the interface between blocks relies on sets of point contacts (Figure 4 and Figure 6). Adjacent blocks can touch along a common edge

segment or at discrete points where a corner meets an edge or another corner. At each contact, the mechanical interaction between blocks is represented by a force (stress), resolved into a normal (F_n or σ_n) and a shear (F_s or τ) component. Contact displacements are defined as the relative displacement between two blocks at the contact point. In the elastic range, contact forces and displacements are related through the contact stiffness parameters (normal and shear).

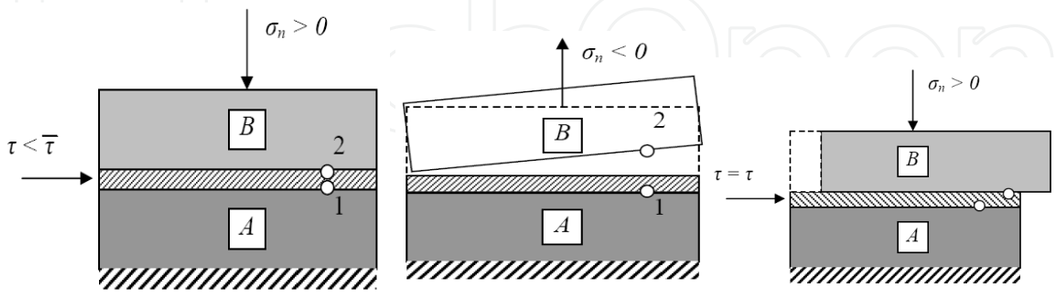

Fig. 4. Coulomb slip model with residual strength (shear and normal behavior).

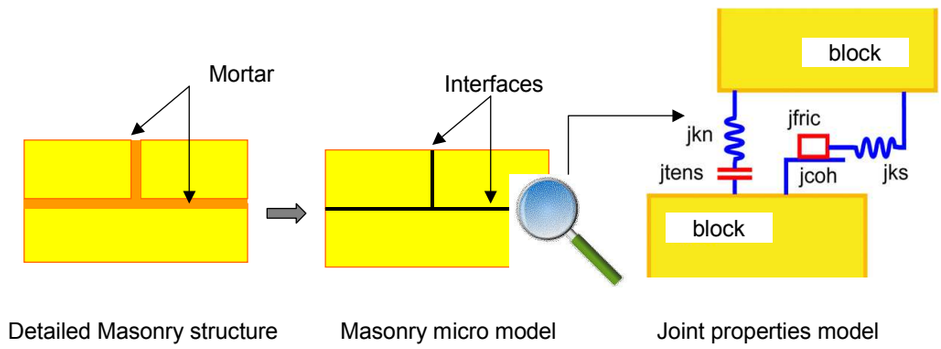

Fig. 5. Interface model code (jkn: joint normal stiffness, jks joint shear stiffness, jcoh: joint cohesion, jfric: joint friction angle and jtens joint tensile strength) (Idris et al, 2009).

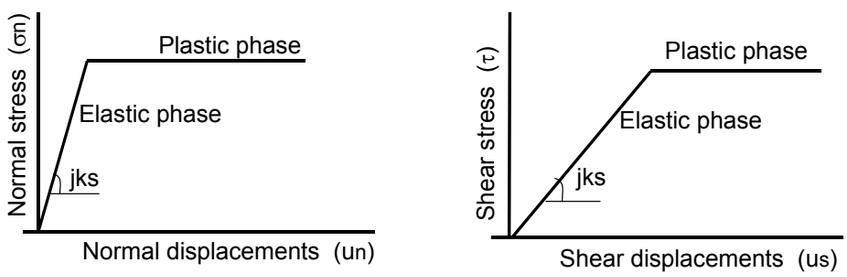

Fig. 6. Joint behavior (respectively) under normal and shear loads.

The mechanical behavior of joints is described as follows, (Itasca, 2000):

- The response to normal loading is expressed by the normal stiffness, jkn and normal displacement Δ un:

$$\Delta\sigma n = jkn\ \Delta un \quad (1)$$

- The shear stress increment is calculated as:

$$\Delta\tau = jks\ \Delta us \quad (2)$$

Where jks, jkn are joint shear stiffness and normal stiffness and Δ us and Δ un are shear displacement and normal displacement of joint. The value of jkn will depends on the contact area ratio between the two joint surfaces and the relevant properties of the joint filing material, if present (Souley, 1993). The value of jks depends on the roughness of the joint surface, which can be determined by the distribution, amplitude, and inclination of the asperities on the friction along the joint, the cohesion due to interlocking, and the strength of the filing material, if present. Figure 5 shows the evolution of joint behavior under normal and shear loads. Figure 6 resume a joint proprieties model for the distinct elements method.

The following parameters are used to define the mechanical behavior of the contacts: the normal stiffness (kn), shear stiffness (ks), friction angle (ϕ), cohesion (c) and tensile strength (R_t). To approximate a displacement-weakening response, the Coulomb slip model with residual strength (Figure 7) is used.

$$\tau = coh + \sigma n \tan fric \quad (3)$$

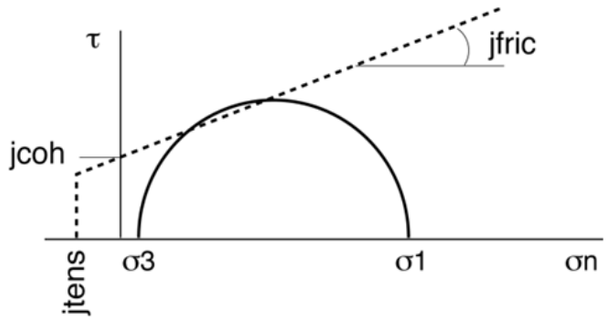

Fig. 7. Elasto-plastic Mohr-Coulomb joint model, code (jcoh: joint cohesion, jfric: joint friction angle and jtens joint tensile strength) (Itasca, 2000, UDEC).

2.3 Calculation method and algorithm

The algorithm of the calculation method for the discrete element method (DEM) must take into account the fact that the geometry of the system, as well as the number and type of contacts between the discrete bodies, may change during the analysis. In the discrete element method the structural analysis, both static and dynamic, is based on explicit algorithms. Among the most important capabilities of DEM that make it very suitable for masonry structures could be mentioned: the ability to simulate progressive failure associated with crack propagation; the capability of simulating large displacements/rotations between blocks; the fact that contact points are updated automatically as block motion occurs and the fact that the problem of interlocking is overcome by automatically rounding the corners.

The calculations performed in DEM alternate between applications of a force and displacement law at all contacts and Newton's second law at all blocks. The force-displacement law is used to find contact forces from known (and fixed) displacements.

Newton's second law gives the motion of the blocks resulting from the known (and fixed) forces acting on them. If the blocks are deformable, motion is calculated at the grid points of the triangular finite-strain elements within the blocks. Then, the application of the block material constitutive relations gives new stresses within the elements. Figure 8 schematically shows the calculation cycle for the distinct element method.

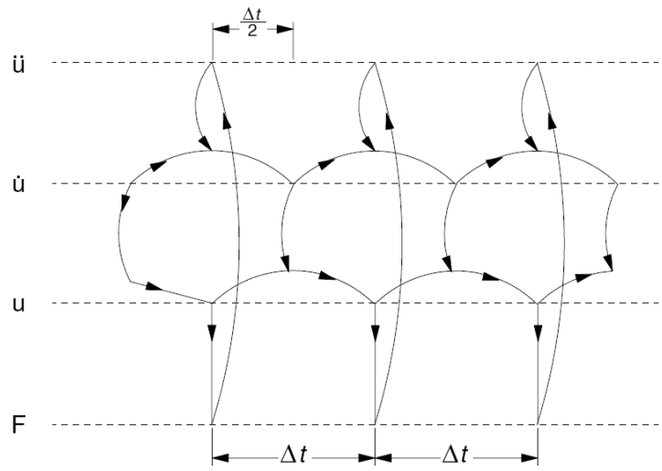

Δt: time step, U: Displacement, Ü: Acceleration, U: Velocity, F: Force

Fig. 8. Calculation cycle used in distinct element formulation (Itasca, 2000).

The motion of an individual block is determined by the magnitude and the direction of resulting out-of-balance moment and forces acting on it. Consider the one-dimensional motion of a single mass acted on by a varying force, *F(t)*. Newton's second law of motion can be written in the form

$$\frac{d\dot{u}}{dt} = \frac{F}{m} \tag{4}$$

where $\dot{u}$ = velocity; t = time; and m = mass.

The central difference scheme for the left-hand side of Eq. (4) at time t can be written as

$$\frac{d\dot{u}}{dt} = \frac{\dot{u}^{(t+\frac{\Delta t}{2})} - \dot{u}^{(t-\frac{\Delta t}{2})}}{\Delta t} \tag{5}$$

Substituting Eq. (5) in Eq. (4) and rearranging yields

$$\dot{u}^{(t+\frac{\Delta t}{2})} = \dot{u}^{\left(t-\frac{\Delta t}{2}\right)} + \frac{F^{(t)}}{m}\Delta t \tag{6}$$

With velocities stored at the half-time step point, it is possible to express displacement as

$$u^{(t+\Delta t)} = u^{t} + \dot{u}^{\left(t+\frac{\Delta t}{2}\right)}\Delta t \tag{7}$$

Because the force depends on displacement, the force/displacement calculation is done at a one-time instant. Figure 1.4 illustrates the central difference scheme with the order of calculation indicated by the arrows. The central difference scheme is "second-order

accurate" — i.e., first-order error terms vanish from the solution. This is an important characteristic that prevents long-term drift in a distinct element simulation. For blocks in two dimensions that are acted upon by several forces as well as gravity, the velocity equations become:

$$\dot{u}_i^{(t+\frac{\Delta t}{2})} = \dot{u}_i^{\left(t-\frac{\Delta t}{2}\right)} + \left(\frac{\sum F_i^{(t)}}{m} + g_i\right)\Delta t \tag{8}$$

$$\dot{\theta}_i^{(t+\frac{\Delta t}{2})} = \dot{\theta}_i^{\left(t-\frac{\Delta t}{2}\right)} + \left(\frac{\sum M_i^{(t)}}{I}\right)\Delta t \tag{9}$$

where $\dot{\theta}$ = angular velocity of block about centroid;
I = moment of inertia of block;
ΣM = total moment acting on the block;
$\dot{u}_i$ = velocity components of block centroid; and
g_i = components of gravitational acceleration (body forces).

In Eq. (9) and those that follow, indices i denote components in a Cartesian coordinate frame, and summation is implied for repeated indices in an expression. The new velocities in Eq. (9) are used to determine the new block location according to:

$$x_i^{(t+\Delta t)} = x_i^{(t)} + \dot{u}_i^{(t+\frac{\Delta t}{2})}\Delta t \tag{10}$$

$$\theta_i^{(t+\Delta t)} = \theta_i^{(t)} + \dot{\theta}_i^{(t+\frac{\Delta t}{2})}\Delta t \tag{11}$$

Where θ = rotation of block about centroid; and
x_i = coordinates of block centroid.

In summary, each timestep (Δt) produces new block positions that generate new contact forces. Resulting forces and moments are used to calculate linear and angular accelerations of each block. Block velocities and displacements are determined by integration over increments in time. The procedure is repeated until a satisfactory state of equilibrium or continuing failure results. Mechanical damping is utilized in the equations of motion to provide both static and dynamic solutions. Gridpoint forces are obtained as a sum of three terms:

$$F_i = F_i^z + F_i^c + F_i^l \tag{12}$$

F_i^l is the external applied loads.

F_i^c is resulted from the contact forces and exists only for gridpoints along the block boundary. Finally, the contribution of the internal stresses in the zones adjacent to the gridpoint is calculated as:

$$F_i^{(z)} = \int_c \ \sigma_{ij}\ n_j\ d_s \tag{13}$$

where σij is the zone stress tensor; and nonlinear and post-peak strength models are readily incorporated into the code in a direct way without recourse to devices such as equivalent stiffness or initial strains. In an explicit program, however, the process is much simpler —

after each time step, the strain state of each zone is known. The program then needs to know the stress in each zone in order to proceed to the next time step. The stress is uniquely defined by the stress-strain model whether it is a linearly elastic relation or a complex, nonlinear and post-peak strength model.

The basic failure model for blocks is the Mohr-Coulomb failure criterion with a non-associated flow rule. Other nonlinear plasticity models available in *Distinct Element codes (UDEC, 3DEC)* are the Drucker-Prager failure criterion, the ubiquitous joint model and strain-softening models for both shear and volumetric (collapse) yield.

2.4 Data limited problems and numerical modeling recommendations

It is necessary when data are limited to measure the quality and the quantity of available data in order to help the understanding of the problem to be solved. In soil-structure interaction and in many other branches of engineering geology, this is a category with limited data available. In this case, it is necessary before starting to be clear on why we are building the model; a good conceptual model can lead to savings in time and money on field tests that are better designed, and then a first model to identify with realistic data and then analyzing the mechanism of the problem, the visualization and the analysis help to understand the behavior of the model. Once we have learned all we can from the simple model or models, then a more complex model can be used. We apply this methodology in this paper.

3. Tunnel masonry structure support proposed models

The first case study (Idris et al, 2009) concerns the simulation of the behavior of an underground structure (Figure 9): old tunnel supported by masonry of stone elements, through this example, we insist on the importance of discontinuities behavior and their characterization (friction angle and cohesion). A majority of the world's tunnels are currently more than 100 years old; these would all be considered as ancient infrastructure. Old tunnels are often supported by a masonry structure. The type of masonry support or lining depends upon utilization of the high compressive strength in the stones, which explains the vaulted section shape of old tunnels supported by masonry.

Old underground constructions, especially tunnels, display specific characters regarding behavioral evolution over time. Infrastructure environment, surrounding ground and used construction materials all contribute to this evolution. Apart from the environment and evolution in surrounding soil and in the absence of an effective isolation system for such underground structures, subsoil water can easily penetrate the masonry joints and circulate within. Over time and in the presence of other aggressive ambient factors, several physical, chemical and biological processes may develop inside the masonry structure; this phenomenon and its impact are collectively called the tunnel-ageing phenomenon. One impact is the alteration in mechanical properties of construction materials (masonry structure composed of blocks and mortar). As a result, various types of disorders appear inside old tunnels (Figure 9); these would include: longitudinal or transverse structural cracks, convergence and partial masonry collapse. The instability of old tunnels depends on the interaction between soil, tunnel support (blocks and mortar).

The study focuses on the evolution of masonry support joint mechanical behavior in built tunnels over time. This study is carried out with the help of the experimental design strategy and numerical modeling by the well-known Universal Distinct Element Code (UDEC).

A tunnel masonry structure is a discontinuous medium consisting of blocks bonded to each other by mortar; in addition, such a structure forms an interface with the surrounding soil. The Distinct Element Method (DEM) is a suitable technique for modeling these structures. By means of the Universal Distinct Element Code (UDEC), a simplified micro-model of an ancient tunnel has been derived (Idris et al., 2009), (Figure. 10). The representative model is positioned at a shallow depth of 20 m. The masonry-supporting section consists of a regular rectangular and square limestone blocks (Figure. 10). Masonry blocks are bonded by lime mortar. The masonry support thickness is 80 cm and the sidewall height amounts to 3 m. By taking into account model section symmetry, only half of each set-up needed to be modeled.

Fig. 9. Illustration and examples of degradations of masonry tunnels.

The soil surrounding the tunnel consists of a homogeneous mix of clay and sand (Verdel and Bigarre, 1999). Table 1 lists the basic mechanical properties assigned to the surrounding soil, masonry and masonry joints, based on the work by Verdel and Bigarre (1999), Hoek (2000) and Janssen (1997).

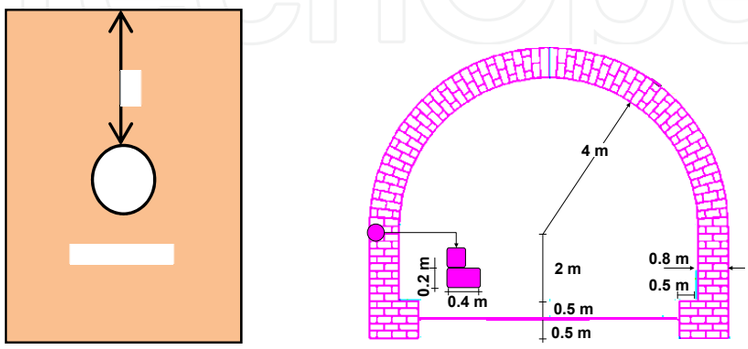

Fig. 10. Old tunnel model using Universal Distinct Element Code UDEC.

Surrounding ground			Masonry			Masonry joints		
Param.	*Unit*	*Value*	*Param.*	*Unit*	*Value*	*Param.*	*Unit*	*Value*
M	Kg/m^3	1900	*M*	Kg/m^3	2000	*jkn*	GPa/m	150
E	MPa	200	E	MPa	6000	jks	GPa/m	69.7
ν		0.3	ν		0.2	jcoh	MPa	1.2
C	MPa	0.50	C	MPa	3	jfric	°	25
φ	°	20	φ	°	30	jtens	MPa	0.4
Tr	MPa	0.10	T	MPa	1			

M: Volumic mass; E: Young modulus; ν: Poisson's ratio; C: Cohesion; φ: Friction angle; T: Tensile strength;
jkn, jks: Normal, tangential joint stiffness; jcoh: Joint cohesion; jfric: joint friction angle; jtens: joint tensile strength

Table 1. Mechanical properties choice of surrounding ground and masonry.

Calculations were carried out in plane strain: the soil and masonry follow a perfect elasto-plastic Mohr–Coulomb plasticity criterion. The calculation step was proceeded by two main stages: model consolidation in the initial stress condition prior to tunnel excavation; and tunnel excavation and simultaneous installation of masonry support. The calculation could then be continued until reaching model equilibrium.

3.1 Ageing simulation of masonry joints in built tunnels

This part of our study sought to understand the evolution in masonry joints behavior over time and evaluate the influence of certain masonry joint mechanical properties on the behavior of masonry old tunnels and the surrounding ground. To simplify the simulation of the complex ageing phenomenon, the strategy has consisted of utilizing experimental designs and response surfaces in combination with various data analyses in order to identify the most powerful experimental factors influencing joint masonry structure behavior over time. A factorial experiment entails a statistical study in which each observation is categorized according to more than one factor. Such an experimental set-up makes it possible to study the effect of each factor on the response variable, while requiring fewer observations than when conducting separate experiments for each factor independently. It also allows studying the effect of the interaction between factors on the response variable (Barrentine, 1999).

In this study, two different experimental designs were proposed to simulate the evolution of mechanical properties of joints. The first experimental design explains the evolution of joints filling material properties and the second explains the evolution of ratio (normal stiffness/ shear stiffness).

3.2 First proposed experimental design

Many factors may influence joint mechanical behavior parameters. In order to predict the 'potential behavior' of the joints under loading, three distinct joint parameters must be introduced into the analysis (Goodman et *al.*, 1968):

- The unit stiffness across the joint, jkn, which characterizes the elastic phase behavior;
- The unit stiffness along the joint, jks, which characterizes the elastic phase behavior;

- Joint fill material proprieties (cohesion, tensile strength, friction angle).

The first experimental design represents the evolution of joint cohesion, joint tensile strength, and joint friction angle. To evaluate the influence of each chosen factor on masonry structure behavior, it proved necessary to observe significant changes in model behavior once factor values had been changed.

Two significant response factors were detected; herein is the cumulated length of open joints and the cumulated length of joints at limiting friction (slip joints). Open joint means that the induced tension stress is greater than joint tension strength and slip joint means the shear strength is less than the induced shear stress using Mohr-Coulomb criteria.

For this purpose, a complete factorial design was proposed; this three-level design is written as K^n factorial design (with K = 3: the studied factor number, n: level number). This nomenclature means that three factors are considered, each one at three distinct levels (Barrentine, 1999). Consequently, a complete factorial design with 27 experiments was proposed. Table 2 contains all of the experimental results (i.e. changed experimental factors and observed responses). In all simulations, soil and masonry blocks properties have been given the unchanged values shown in Table 2.

Surrounding ground				Masonry		Masonry joints		
Param.	Unit	Value	Param.	Unit	Value	Param.	Unit	Value
M	Kg/m3	1900	M	Kg/m3	2000	jkn	GPa/m	5
E	MPa	100	E	MPa	10000	jks	GPa/m	2
ν		0.3	ν		0,3	jcoh	MPa	1
C	MPa	0.1	C	MPa	6	jfric	°	40
φ	°	30	φ	°	60	jtens	MPa	0
Tr	MPa	0.10	Tr	MPa	3			

M: Volumic mass; E: Young modulus; ν: Poisson's ratio; C: Cohesion; φ: Friction angle; T: Tensile strength; jkn, jks: Normal, tangential joint stiffness; jcoh: Joint cohesion; jfric: joint friction angle; jtens: joint tensile strength

Table 2. Characterization of soil, blocs and joints of masonry.

Figure 11 and Figure 12 provide some selected results, which show the influence of joint parameters on the length of open and slip joint evolution on mechanical behavior of masonry support structure.

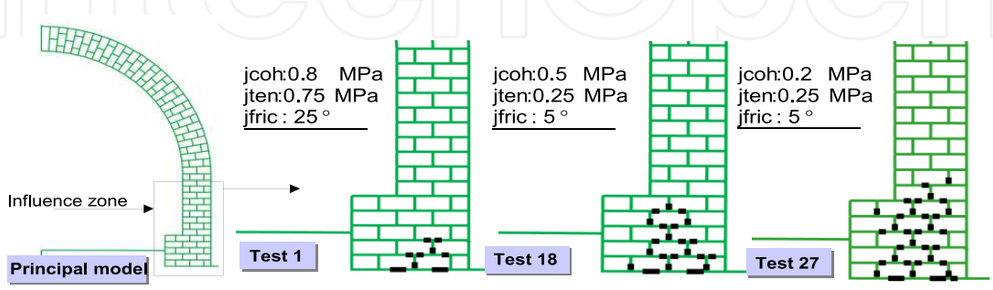

Fig. 11. A sample of numerical simulation results; the observed response is the total length of open joints (σ_n<JR_T).

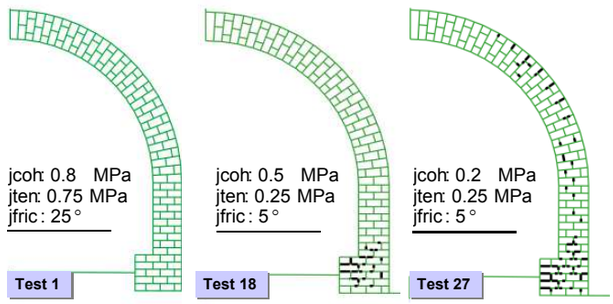

Fig. 12. A sample of numerical simulation results, the observed response is the total length of joints at limiting friction (slip joints).

3.3 Response surface analysis

To summarize the experimental design results, 3D graphical response surfaces were generated, where the predicted responses (cumulated length of open joints and cumulated length at limiting friction) were indicated by a plane surface distance that relates every pair of modified factors (Kresic, 1997). These response surfaces yield a graphical indication of the reliability of results obtained; they also make it possible to compare dual influences from the studied factors and to observe possible interactions between them (Figure. 13 and Figure. 14).

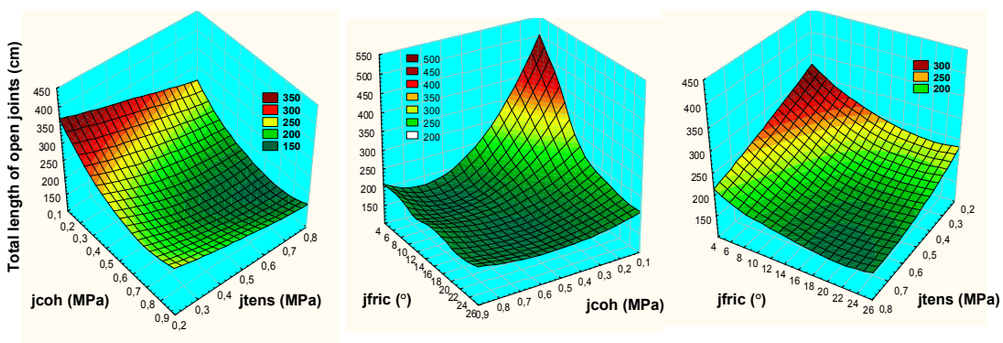

Fig. 13. Response surfaces for relating the total length of open joints with the data set (jcoh: joint cohesion, jtens: joint tensile strength and jfric: joint friction angle).

Response surface (Figure. 14) analysis highlights a number of key points:

The joint cohesion has a higher influence than joint tensile strength on the cumulated length of open joints.

- The evolution in two factors together (joint cohesion and joint friction angle) exerts remarkable influence on masonry block mechanical behavior (i.e. on the cumulated length of open joints) which means that these two parameters have an important interaction influence on the observed response.
- The difficulty is in comparing the influence of joint cohesion with that of joint friction angle on the mechanical behavior of masonry.

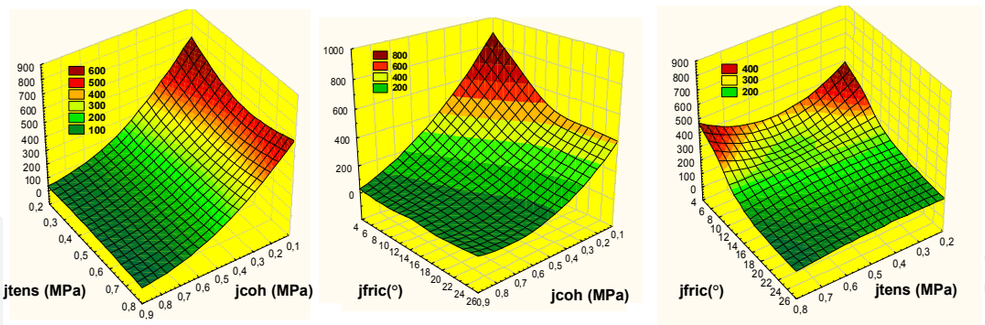

Fig. 14. Response surfaces for relating the total length of joints at limiting friction with the data set (jcoh: joint cohesion, jtens: joint tensile strength and jfric: joint friction angle).

3.4 Second proposed experimental design

The determination of jkn and jks is a complex operation and many authors propose experimental studies. The second experimental design expresses just the evolution of the ratio (jkn/jks) to evaluate its influence on masonry structure behavior, where:

- jkn is joint normal stiffness;
- jks is joint shear stiffness.

The (jkn/jks) ratio may exceed 100 (Souley, 1993), so this experimental design suggests that the ratio (jkn/jks) changes between 2 and 100, where jkn remains constant and only jks changes its value. It proved necessary to observe significant changes in model behavior once the (jkn / jks) ratio had been changed. The observed response in this step of the study is the total length of shear displacements detected on the tunnel masonry support section after every modeling test. Table 3 provides the detailed experimental design and the obtained results. This experimental design contains 12 modeling tests. Figure 15 provides some selected results, which show the influence of (jkn/jks) ratio evolution on mechanical behavior of masonry support structure.

Figure 16 shows the relations between (jkn/jks) ratio and observed response of the cumulated length of joint shear displacements. On figure 16, we can distinguish a remarkable rapid increase in the total length of joint shear displacements when the (jkn/jks) ratio varies between 2 and 20.

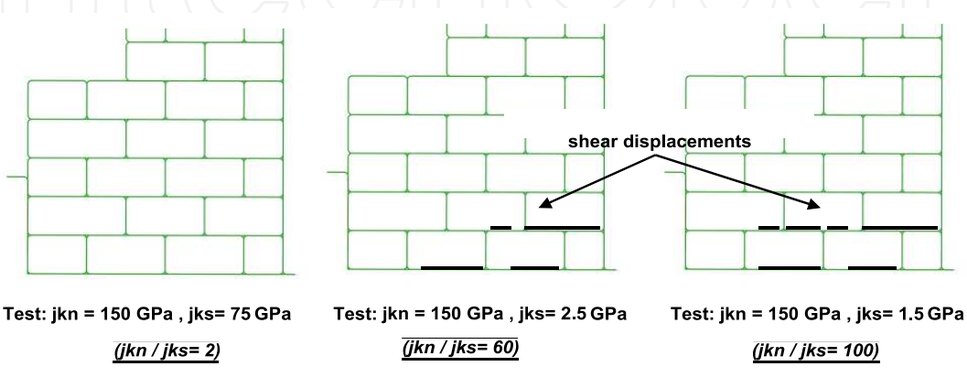

Fig. 15. Some numerical simulation results examples.

After that, the relation between the (jkn/jks) ratio and the cumulated length of joint shear displacements seems to be a linear relation and the cumulated length of joint shear displacements seems to increase slightly with the rise of the (jkn/jks) ratio more than 20. We can extract from the previous analysis that the (jkn /jks) ratio increases and directly influences the behavior of masonry support structure in old tunnels by the increase of shear displacement along affected joints.

3.5 Influence of masonry joint proprieties evolution on the surrounding ground of tunnel

The evolution of mechanical joint parameters (jcoh, jten, jfric, jkn and jks) did not have any significant influence on the mechanical behavior of the surrounding soil. The significant evolutions concern only the masonry joint behavior. Generally, in old tunnels, the use of the masonry support is strong enough, the models inspired from real built tunnels, with 80 cm of masonry support which have very strong support. Masonry structure is mainly loaded in compression due to its vaulted section shape. This massive support may explain the absence of block mechanical parameters that influence the behavior of surrounding soil (Idris et *al.*, 2008).

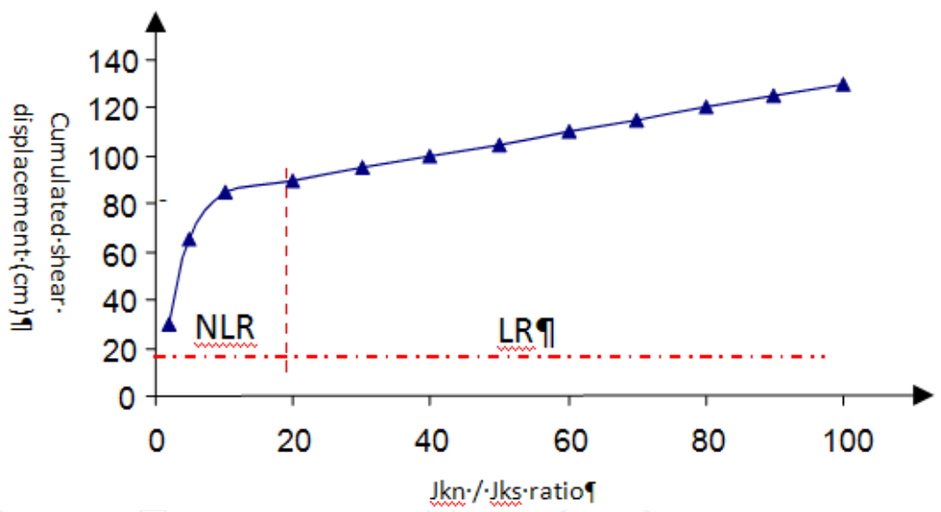

NLR: Non Lenar Relation LR: Linear Relation, Jkn : Joint normal stiffness, Jks : Joint shear stiffness

Fig. 16. Graphical presentation of shear displacements as a function of the jkn/jks ratio.

3.6 Conclusion

The study concerned the behavior of masonry tunnel structures due to the ageing phenomena by using numerical modeling and experimental design. A first experimental design was proposed to simulate ageing effects of old tunnel behavior; a complete factorial experimental design, which expresses the evolution of three selected masonry joints mechanical properties, was then forwarded. The factors selected for the present study were: masonry joint cohesion, joint tensile strength and joint friction angle. All experimental design tests were modeled by means of the distinct element method. Two significant responses were detected, they are respectively: the total length of open joints; the total length of joints at limiting friction (slip joints).

An analysis of results indicated that the three studied masonry joint mechanical factors have significant influence on masonry mechanical behavior expressed by the total length of open joints. Joint cohesion is the most important factor, then joint tensile strength and finally joint friction angle. Only the interaction of joint cohesion and joint friction angle have significant influence on the total length of open joints. For the total length of joints at limiting friction, only joint cohesion and joint friction angle have a significant influence and joint cohesion remains the most important factor. These two factors have a significant interaction influence on the mechanical behavior of tunnel masonry support.

The second proposed experiment design expressed the evolution of the ratio jkn/jks. The detected significant response was the total length of shear displacements along masonry joints. Results showed that shear displacements increase according to jkn/jks ratio increase. The total length of shear displacements evolution follows two types of relations as a function of the jkn/jks ratio; firstly it follows a non-linear relation according to certain jkn/jks values (jkn/jks=[2-20]), then it changes (increases slightly) behavior according to a linear model.

4. Impact of underground movement on a masonry wall

The second case study concerns in particular the behavior of a masonry wall under the effect of an underground excavation (tunnel, mine, soil settlement, etc.). The main objective is to verify and to improve the comprehension of masonry structure behavior using the numerical modeling approach by distinct element method.

The excavation of tunnels and underground mines modifies the initial stress distribution and induces displacements on the ground surface (Peck, 1964, Standing, 2008, Al Heib, 2008). Figure 17 diagrammatically shows the surface subsidence trough above an advancing tunnel. The surface subsides and structures can be damaged due to the induced strains (Figure 17). For 'Greenfield sites', i.e. those without the presence of buildings or subsurface structures, the shape of this trough transverse to the axis of the tunnel closely approximates to a normal Gaussian distribution curve - an idealization which has considerable mathematical advantages. The subsidence trough consists of vertical and horizontal displacements.

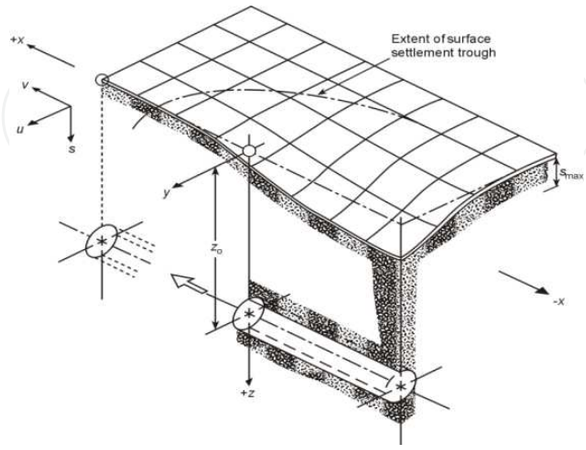

Z_0: depth of the tunnel, S_{max}: maximum subsidence

Fig. 17. Surface settlement above an advancing tunnel (Standing and Burland, 2008).

The amount of damage caused by subsidence depends upon the magnitude and the type of ground movements, structural factors and geological factors (Burland, 1995, Standing and Burland, 2008). The magnitude of ground movements on the structure are governed by its location and orientation in relation to the underground workings and the depth of underground cavities (Figure 18).

Fig. 18. Damages induced by compression strain due to soil subsidence (Deck et al., 2003).

4.1 Damage due to horizontal strain

The different types of movements can affect structures in different ways (Figure 19). Vertical subsidence may affect tall buildings (local tilt) and long buildings (deferential settlements). Horizontal extension and compression strain, tilt and curvature are the causes of the most commonly seen type of subsidence damages. Damage to buildings is generally caused by differential horizontal movements (horizontal strain) and the concavity and convexity of the subsidence profile. The extension horizontal strain is characterized by the fracturing of the masonry and the compression strain is characterized by squeezing-in of voids (doors and windows). Unlike settlements, there are fewer case histories where horizontal movements have been measured. The maximal horizontal displacement depends on the soil behavior and the geometry of the excavations; it generally equals 40% of the maximal vertical displacement (Lake et al, 1998). Horizontal displacements can be differentiated to give the horizontal strain ε_h at any location on the ground surface.

4.2 Building damage assessment and soil-structure interaction

It is clear from the above, considering tunnel construction and underground excavation, even with Greenfield conditions, that precise prediction of ground movements due to ground excavation is not realistic. However, it is possible, *for non-stiff buildings*, to make reasonable estimates of the likely range of movements provided excavation is carried out under the control of suitably qualified and experienced engineers and highlighted by numerical and physical modeling (Standing and Burland, 2008).

Building deformation and its potential damage caused by subsidence in urban areas has a major impact on the planning and construction process of any underground excavation. The use of Greenfield subsidence parameters to determine the level of the damages appears as a conservative approach; it can lead to costly projects. Potts and Addenbrooke (1997) and others (Dimmok et al, 2008) introduce design charts for tunnels to consider the influence of the buildings own stiffness, thus leading to more realistic predictions of induced deformations. The approach introduced by Potts and Addenbrooke was based on

continuous and simplified 2D numerical modeling. The building was modeled by weightless, elastic beams. Franzius (2004) presented the results of an extensive parametric study using 3D FE analysis. The relative stiffness expressions were introduced to relate the stiffness of a surface structure to the stiffness of the ground; they defined the relative bending and axial stiffness respectively:

$$\rho^* = \frac{EI}{E_s(\frac{B}{2})^4} \text{ and } \alpha^* = \frac{EA}{E_s(\frac{B}{2})} \quad (14)$$

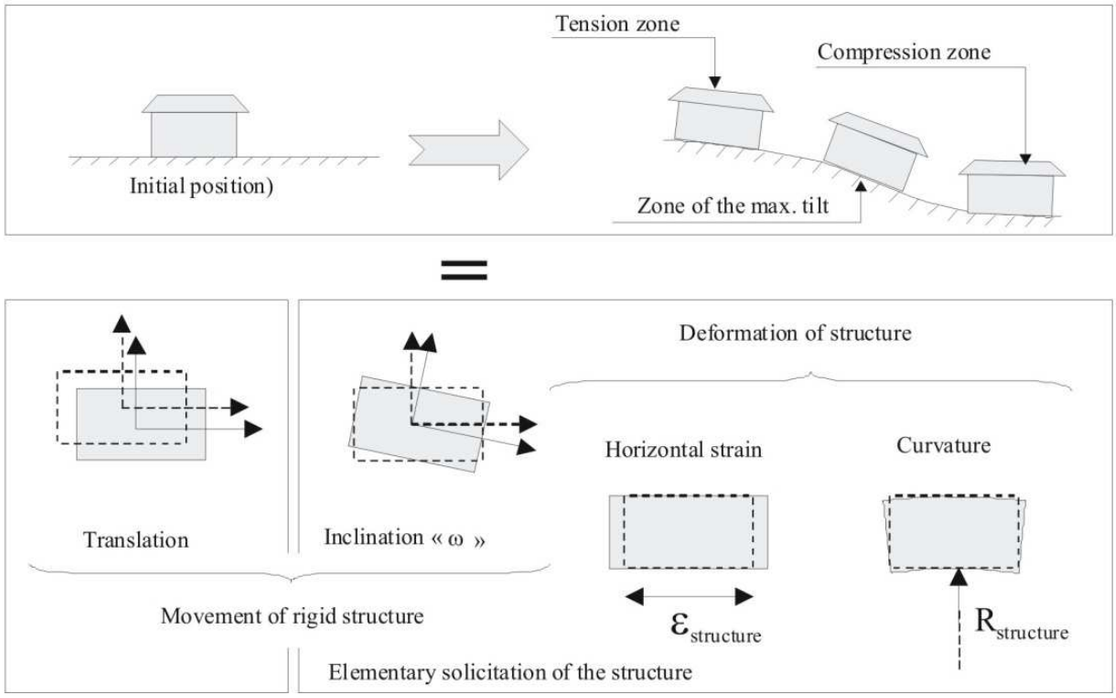

Fig. 19. Transfer surface movement to the surface structure (Deck et al, 2003).

Son and Cording (2007) had evaluated the stiffness for a masonry building using the distinct element code UDEC, their studies were limited to evaluating the influence of Young modulus and shear modulus for different value parameters and taking into account the presence of windows and doors. Giorgia Giardina et al (2008), studied masonry wall damaging due to tunneling; they confirm, using finite elements, that the Greenfield approach is too conservative, and that the total interaction (coupling) approach is more realistic but needs more time and energy to obtain the results. The masonry wall is generally very vulnerable due to the compression strain and shear strain as shown in the pictures. The failure generally appears along the mortar joints around openings corresponding to weakness zones of the walls. To study the effect of soil-structure interaction and the role of the stiffness due to the horizontal strain, we consider the numerical modeling approach.

4.3 Numerical model description

The present work is focused on the behavior of a masonry wall under horizontal strain. In addition to the evaluation of the stiffness of the masonry wall, the objective of the numerical

modeling is to quantify the movement transfer from the soil to the masonry structure. The class of the wall damage depends on the characterization of the wall: geometry and proprieties. The 3D numerical models use the distinct elements code (3DEC). The model presents an individual wall of unreinforced masonry; the wall is under only the effect of the horizontal displacements and dead load. The horizontal displacements were applied on the boundary of soil (model). The masonry wall dimensions are: 10 m length, 5 m high and 25 cm thick. The wall consists of masonry units of 50 cm * 25 cm * 25 cm (reference). Two configurations were studied with and without windows. The model has two parts: the soil and the wall, the soil behavior is considered as elastic-plastic, homogenous and isotropic. The plastic criterion (failure) is the Mohr-Coulomb defined by cohesion and friction angle,

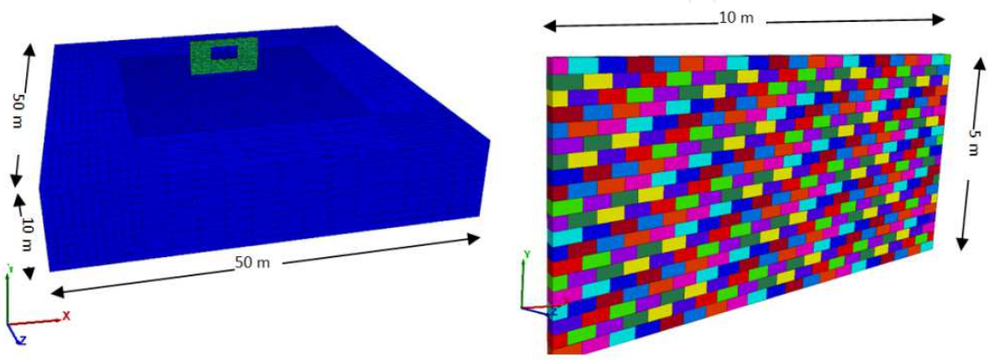

Fig. 20. 3DEC numerical model using distinct element method for ISS.

The behavior assumption of masonry units is as elastic and isotropic material. The mortar between blocks corresponds to vertical and horizontal joints. The behavior of the joints is considered as elastic-plastic and the plastic criterion is Mohr-Coulomb which is defined by the friction angle, the cohesion and the tensile strength. The table presents the priorities of soil, blocs and joints of masonry. Table 1 lists the basic mechanical properties assigned to the soil, the masonry and the masonry joints; they are based on the estimations from different international publications. The characterization of soil and building are very close to those used by Potts and Addenbrooke. The calculation was divided into two main stages: the stage of the consolidation to obtain the initial stress condition and the application of the horizontal displacements on the lateral boundary surface. The calculation could then be continued until reaching model equilibrium. Two directions of displacement were studied. The first one corresponds to in-plane solicitation and the second one corresponds to out-plane. The boundary condition of the horizontal displacement induced in the soil a compression horizontal strain in Greenfield equal to 8 mm/m.

4.4 Evaluation of relative stiffness of the wall

Two assumptions were employed to quantify the relative stiffness according to the relation introduced by Potts and Addenbrooke (1996): the first one considers the wall as a continuous single bloc and the second assumption considers the wall as an assembly of masonry units (Figure 21). The following relations (Figure C) determine the equivalent Young modulus (E_1, E_2) and the equivalent shear modulus (G_{12}) taking into account the geometrical and mechanical parameters of discontinuities for the second assumption. The second assumption reduces the stiffness of the wall.

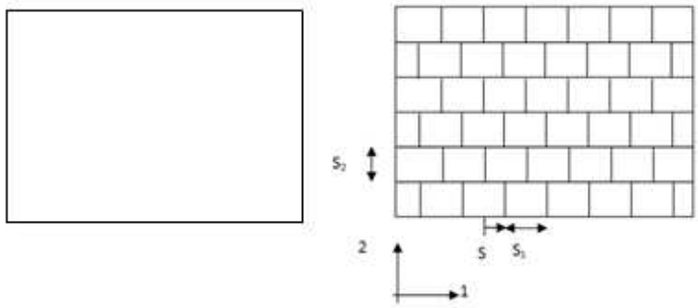

a- Single bloc Masonry blocs

$$E_1 = \frac{E}{1 + \frac{B_{n1} E}{S_1 \; K_{n1}}} \qquad \nu_1 = \frac{\nu}{1 + \frac{B_{n1} E}{S_1 \; K_{n1}}}$$

$$E_2 = \frac{E}{1 + \frac{E}{S_2 \; K_{n2}}} \qquad \nu_2 = \frac{\nu}{1 + \frac{E}{S_2 \; K_{n2}}}$$

$$\frac{1}{G_{12}} = \frac{1}{G} + \frac{B_{t1}}{S_1 \; K_{S1}} + \frac{B_{t2}}{S_2 \; K_{S2}}$$

With

$$B_{t1} = \left[1 + \frac{K_{n2} \; S}{K_{s1} \; S_2} \left(1 - \frac{S}{S_1} \right) \right]^{-1}$$

$$B_{n1} = \left[1 + \frac{K_{s2} \; S}{K_{n1} \; S_2} \left(1 - \frac{S}{S_1} \right) \right]^{-1}$$

E_1, E_2 : Young modulus, ν_1, ν_2: Poisson ratio,
G_{12}: Shear modulus, S1,S2: horizontal and vertical spacing.

c- equivalent elastic parameters

Fig. 21. Assumptions for determining the relative stiffness of the masonry wall.

Table 3 lists the parameters assigned to the wall and the estimated axial and flexion stiffness of the masonry wall.

Continue Wall			Masonry wall		
Parameter	*Unit*	*Value*	*Parameter*	*Unit*	*Value*
I	***m^4***	***32e-4***	***I***	***m^4***	***32e-4***
A	***m^2***	***0.125***	***A***	***m^2***	***0.125***
E	MPa	10000	*E*	MPa	2000
EI	MNm^2	32	EI	MNm^2	2156
Es	MPa	100	Es	MPa	100
B	m	10	B	m	10
ρ*	°1/m	83	ρ*	°1/m	17
α*		100	α*		21.56

I: Volumetric mass; E: Young modulus;

Table 3. Wall stiffness calculation according to the Potts and Addenbrooke approach.

Observing the charts which were introduced by Potts and Addenbrooke (Figure 22), the studying wall is stiff enough and the transfer of soil deformations to the wall is small, may be equal to zero for all structure positions from the position of the underground excavation (e/B). The adopted approach by Potts and Addenbrooke is very simplified for a masonry wall and the realistic behavior can be suspected as completely different from the above conclusions according to in-situ observations.

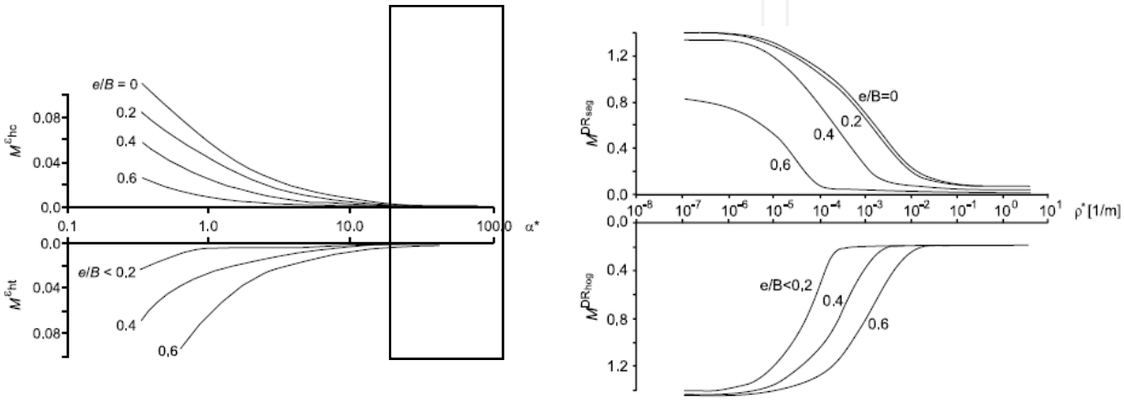

Fig. 22. Chart for determining the strain (ε and D) transfer from soil to structures function of relative axial α and flexion ρ stiffness.

4.5 Results analysis

The analysis of results will be limited to the behavior of the masonry wall due to the effect of the horizontal displacements (horizontal strain). We looked for the state of joints (mortar): elastic, open or sliding; and the horizontal and vertical displacements of the wall. We compare the horizontal strains of the masonry wall to the horizontal strain of the soil under Greenfield conditions.

The first configuration corresponds to in-plane solicitation without windows. The Figure 23 presents the horizontal and the vertical displacements of the wall. The horizontal displacement direction corresponds to the direction of the solicitation and the vertical displacement direction is oriented toward the top. The distribution of displacements depends on the localization of the cracks due to the failure of vertical joints. A principal discontinuity was formed near the second part of the wall; the principal discontinuity is associated with three or four cracks (joints). The dip of discontinuity is about 45° to 60°. The variation of the horizontal strain decreases from the bottom to the top of the wall. The maximum horizontal strain is 1.4 mm/m. The transfer of the horizontal strain from soil to the wall is equal to 17.5%.

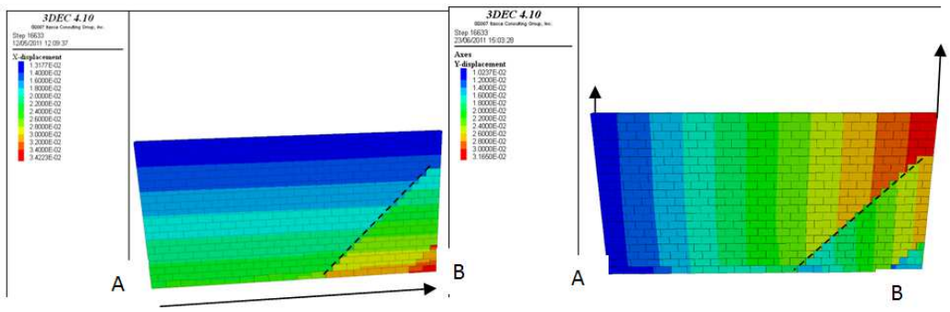

Fig. 23a. Horizontal and vertical displacements of the wall.

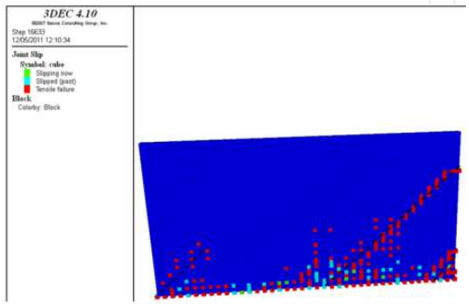

Fig. 23b. Failure of the joints creating inclined and vertical cracks.

The second configuration corresponds to the introduction of a window in the centre of the masonry wall, which surface corresponds to 16% of the wall surface. The presence of a void in the wall modifies the distribution of the displacements and the localization of the cracks (Figure 24). The horizontal strain increases and it is equal to 2.65 mm/m instead of 1.4 mm/m, the transferred strain is equal to 33% of soil strain. The stiffness of the wall decreases due to the window, the density of cracks increases also, we observe new cracks in the upper part of the wall above the window zone due to tension stresses. The numerical results are very close to the in-situ observations due to the subsidence.

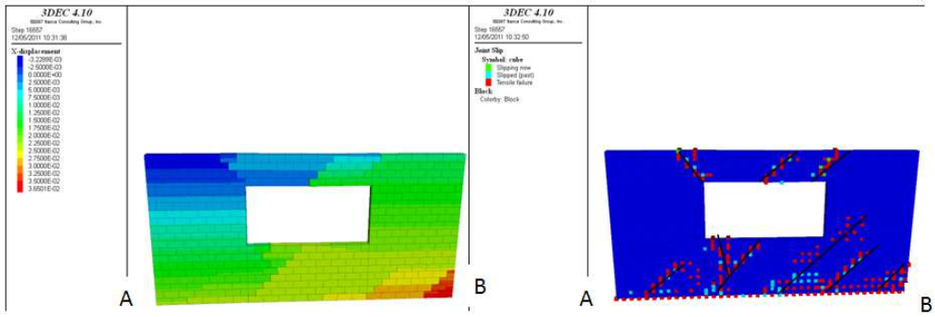

a- Horizontal displacement b- Failure localization

Fig. 24. Behavior of masonry wall under the effect of ground subsidence due to the underground excavation – results obtained by 3DEC numerical model.

The third and the fourth configurations correspond to the horizontal displacement applied perpendicularly to the wall (out-plane). Figure 25 presents the mechanism of the wall

deformation, the displacement of the bottom part of the wall is the opposite of the displacement of the upper part. The behavior of the wall is influenced by the direction of the solicitation and the stiffness of the wall. A horizontal open crack was created by the impact of horizontal displacement point C), the localization of this crack is at 1 m from the base of the horizontal strain between points A and C. It is equal to 100 mm/m, it is much greater than the applied horizontal strain (8 mm/m) on the ground, and in the second part of the wall, and the strain is less than the soil horizontal strain.

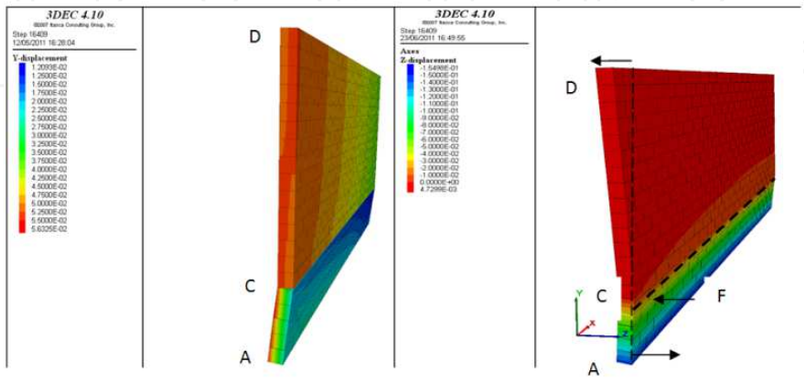

a- Horizontal displacement b- Failure localization

Fig. 25. Behavior of masonry wall under the effect of ground subsidence due to the underground excavation – results obtained by 3DEC numerical model.

The fourth configuration takes into account the presence of the window. The presence of the window increases the number of cracks very strongly. Some blocks lose their contacts because of the free surface and can fall.

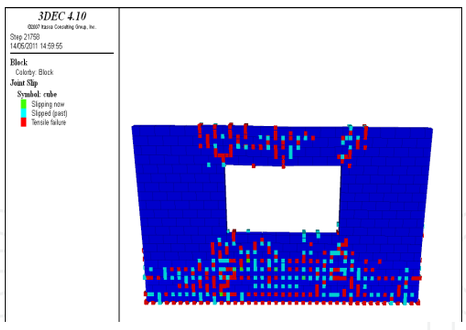

Fig. 26. Behavior of masonry wall under the effect of ground subsidence due to the underground excavation – results obtained by 3DEC numerical model.

Table 4 resumes and compares the values of horizontal displacements (Ux and Zu) and vertical displacement (Uy) and the localization damages according to the behavior of vertical and horizontal joints. Figure 27 presents an interpretation of the wall behavior under the influence of the horizontal strain. The wall is influenced by the ground displacements. This solicitation of the wall by the horizontal strain reveals traction failures in the joints of masonry blocks. These failures can form oblique cracks in the wall along vertical and horizontal mortar.

A ground horizontal strain, in Greenfield conditions, equaling 8 mm/m can induce severe damage on structures according to different prediction methods without the effect of soil-structure interaction (Deck et al., 2003, table 5).

	Ux (mm)	Uy (mm)	Uz (mm)	Localization of damages
In-plane	34	31	4.9	One principal inclined shear crack and many incomplete shear cracks associated with open cracks, with the direction of horizontal displacement.
Out-plane	18	56	-154	Horizontal crack at 1.5 m from the base and distortion and tilt of transversal section
In-plane – window	36		7	Inclined shear cracks associated with open cracks, with the direction of horizontal displacement. Up the window, inclined cracks in the opposite direction
Out-plane - window	11.5	62	144	Distortion of the wall associated to the fall of certain blocks, increase in the number of cracks

Table 4. Displacements and damage localization of masonry wall.

The damages can be determined by the chart of Boscardin and Cording (1989) and Potts and Addenbrooke (1996) and Table 5. In this case, damage must be very severs. The results of numerical modeling using 3D distinct elements code highlights this point and shows this evaluation must be improved taking into acount the interaction between soil and structure and the behavior of joints. The numerical results are strongly close to the physical modeling results obtained by Cox (Cox, 1980) and in situ observations (Deck, 2002).

Limits horizontal strain ε mm/m	< 0.5 for negligible degradations. 0.5 to 0.75 for very light damage. 0.75 to 1.5 for light damage. 1.5 to 3 for moderate damage. > 3 for severe damage.

Table 5. Classes of degradation according to horizontal strain.

5. Conclusion

The study focused on the behavior of the masonry wall due to horizontal deformation of the soil; the study also focused on soil-structure interaction and the movement of transfer of soil structure using numerical modeling. A 3D numerical model of the masonry wall was made to simulate the behavior. The study examined the observance of the level and location of damage due to horizontal deformation of the soil; particular attention was granted to the location of cracks based on the direction of solicitation and the existing window. Different configurations have been calculated and analyzed horizontal and vertical movements.

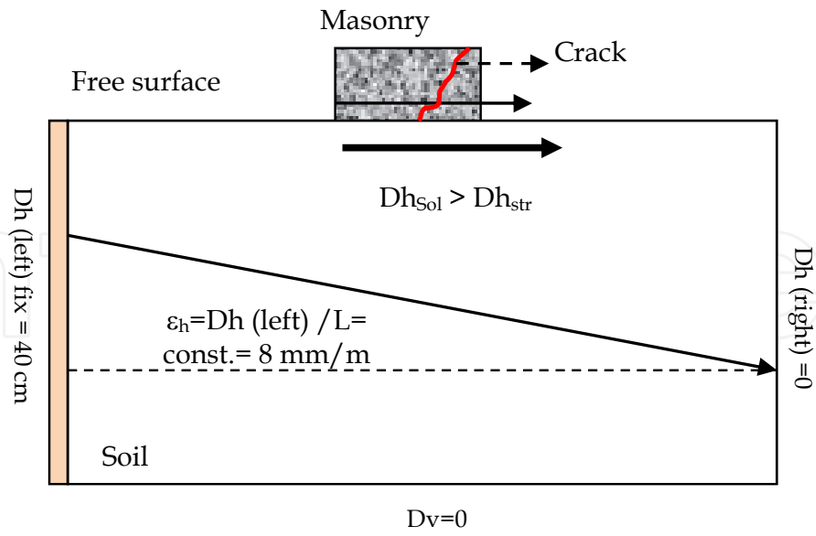

D_h: horizontal displacement, D_v: vertical displacement, ε_h: horizontal deformation

Fig. 27. Analyze of soil structure interaction due to the ground movement.

The resulting analysis indicated that a masonry wall formed by masonry units is more sensitive to horizontal strain than a continuous structure idealized by a beam. We can conclude that the theory of beams and the Potts and Addenbrooke chart underestimate the impact of horizontal strain. The out-plane horizontal strain can seriously damage the masonry wall, with the introduction of a main horizontal crack, the level of damage in this case is more important than the in-plane horizontal solicitation. The presence of a window decreases the stiffness and increases the damage to the wall.

In conclusion, numerical modeling using the distinct element method is an original tool to improve the comprehension of wall damaging; the obtained results are very close to in-situ observations and can supplement an advancing progress for the evaluation of masonry structures.

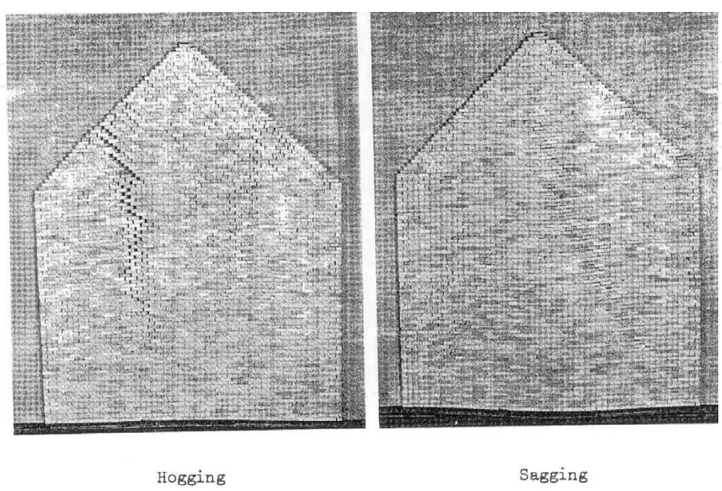

Fig. 28. Effect of horizontal strain on masonry wall using physical modeling (Cox, 1980).

6. References

Al Heib M. (2008). State Of The Art Of The Prediction Methods Of Short And Long-Term Ground Movements (Subsidence And Sinkhole) For The Mines In France. In: Coal Geology Research Progress. ISBN: 978-1-60456-596-6. Editor: Thomas Michel and Hugo Fournier. 2008 Nova Science Publishers, Inc. pp 53-76.

Barrentine, Larry B., (1999). An introduction to design of experiments: a simplified approach. Experiments with Three Factors. The American Society for Quality, pp. 27–35 (Chapter 3).

Boscardin, M.D. and Cording, E.G. (1989). Building response to excavation-induced settlement, *Journal of Geotechnical Engineering*, ASCE, 115(1): 1-21.

Burland, J.B. (1995). Assessment of risk of damage to buildings due to tunneling and excavations. Invited special lecture, in: Proc. 1st Int. Conf. Earthquake Geotechnical Engineering, IS-Tokyo, 1189-1201.

Cox D. W. (1980).- Modeling stochastic behaviour using the friction table with examples of cracked brickwork and subsidence. Proc. of the 2nd international conference on ground movements *and structures*, Cardiff (Avril 1980), Edité par GEDDES J. D., Pentech press, pp. 307-328.

Cundall, P. A., (1971), A computer model for simulating progressive large scale movements in blocky rock systems', in Proc. of the Symposium of the International Society of Rock Mechanics (Nancy, France, 1971), 1, Paper No. II-8.

Deck O., Al Heib M., and Homand F. (2003). Taking the soil-structure interaction into account in assessing the loading of a structure in a mining area. Engineering Structure 25:435-448.

Dimmock, P.S. and Mair R.J. (2008). Effect of building stiffness on tunneling-induced ground movement, Tunneling and Underground Space Technology, 23: 438-450.

Eurocode 6, (1996). Calcul des ouvrages en maçonnerie – Partie 4: Méthode de calcul simplifies pour les ouvrages non armée, NBN EN (1996-3) (ANB).

Franzius, J.N., Potts, D.M., Burland, J.B., (2006). The response of surface structures to tunnel construction, Proc. Inst. Civ. Eng. Geotech. Eng., 159 (1), 3–17.

Giorgia Giardina, Max A.N. Hendriks, Jan G. Rots (2008). Numerical analyses of tunnel-induced settlement damage to a masonry wall. 7th fib PhD Symposium in Stuttgart, Germany

Goodman, R. E., Taylor, R. L., and Brekke, T. L., (1968). A Model for the Mechanics of Jointed Rock, Journal of the Soil Mechanics and Foundations Div., ASCE, Vol. 94, No SM3, pp. 637-659.

Itasca, 2000. UDEC Universal Distinct Elements Code Manual. Continuously yielding joint model. Itasca Consulting Group Inc., pp. 1–16.

Idris J., Al Heib M., Verdel T. (2009). Masonry joints mechanical behaviour evolution in built tunnels. Analysis by numerical modelling and experimental design, Tunnelling and Underground Space Technology, 24 (2009) 617–626.

Janssen, H.J.M., (1997). Structural masonry. In: Balkema, A.A. (Ed.), Numerical studies with UDEC. Centre for civil engineering research and codes. Roterdam, Netherlands, ISBN 90 5410680 8, pp. 96–106.

Hoek, E., (2000). Practical Rock engineering. Rock Mass Properties. rocscience.com on line, Chapter 11, pp. 161–203.

Lourenço, Paulo B., (2002). Guidelines for the analysis of historical masonry structures. University of Minho, Guimarães, Portugal

Kresic, N., (1997). Quantitative Solution in Hydrology and Groundwater Modelling, Inverse Distance to a Power Method. Lewis Publishers, pp.121–123.

Lake L.M., Rankin W.J. and Hawley J. (1992). Prediction and effects of ground movements caused by tunnelling in soft ground beneath urban areas. CIRIA funders report CP/5 129p.

Massart T.J., Peerlings R.H.J., Geers M.G.D., Gottcheiner S., (2005). Mesoscopic modeling of failure in brick masonry accounting for three-dimensional effects. Engineering Fracture Mechanics 72 (2005) 1238–1253

Lemos, J. V. (1998). Discrete Element Modeling of the Seismic Behavior of Stone Masonry Arches," in Computer Methods in Structural Masonry 4 (4th International Symposium, Florence, Italy, September 1997), pp. 220-227, G. N. Pande et al., Ed. London: E&FN Spon.National Coal Board 1975. Subsidence Engineers Handbook. National Coal Board Production Dept., U.K.

Peck, R. (1969). Deep excavations and tunnelling in soft ground, Proceedings of the 7th International Conference on Soil Mechanics Foundation Engineering, Mexico, 3:225-290.

Potts, D.M. and Addenbrooke, T.I. (1997). A structure's influence on tunneling-induced ground movements. Proc. Instn. Civil Engrs., Geotechnical Engineering, 125 : 109-125.

Souley, M., (1993). Modelling of jointed rock masses by distinct element method, influence of the discontinuities constitutive laws upon the stability excavation. Doctoral thesis of (Institut national polytechnique de Lorraine), pp.75-136.

Son M. and Cording E. J. (2007). Evaluation of building stiffness for building response analysis to excavation-induced ground movements. Journal of Geotechnical engineering. ASCE/August 2007 (995-1002).

Standing, J. and Burland, J.B. (2008). Impact of underground works on existing infrastructure, Invited lecture in Post-Mining, France, 1-39.

Sutcliffe D.J., Yu H.S., Page A.W., (2001). Lower bound limit analysis of unrienforced masonry shear walls, Computers and structures, pp. 1295-1312.

Tzamtzis A.D. and Asteris P.G., (2004). FE Analysis of Complex Discontinuous and Jointed Structural Systems (Part 1: Presentation of the Method - A State-of-the-Art Review). Electronic Journal of Structural Engineering, pp. 75-92.

Verdel T., (1994). La méthode des éléments distincts (DEM) : un outil pour évaluer les risques d'instabilités des monuments en maçonnerie. Applications à des cas égyptiens. Actes du Septième Congrès de l'Association Internationale de Géologie de l'Ingénieur, Lisbonne, Septembre 1994, pp 3551-3560, Ed BALKEMA (ISBN 90 54 10 503 8)

Verdel, T. and Bigarre, P. (1999). Modélisation de tunnels anciens avec le logiciel UDEC, Rapport INERIS, Société SIMECSOL, pp. 1-12.

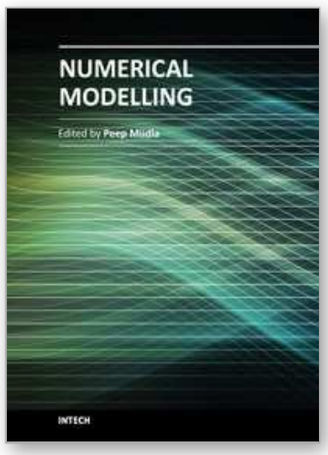

Numerical Modelling

Edited by Dr. Peep Miidla

ISBN 978-953-51-0219-9
Hard cover, 398 pages
Publisher InTech
Published online 23, March, 2012
Published in print edition March, 2012

This book demonstrates applications and case studies performed by experts for professionals and students in the field of technology, engineering, materials, decision making management and other industries in which mathematical modelling plays a role. Each chapter discusses an example and these are ranging from well-known standards to novelty applications. Models are developed and analysed in details, authors carefully consider the procedure for constructing a mathematical replacement of phenomenon under consideration. For most of the cases this leads to the partial differential equations, for the solution of which numerical methods are necessary to use. The term Model is mainly understood as an ensemble of equations which describe the variables and interrelations of a physical system or process. Developments in computer technology and related software have provided numerous tools of increasing power for specialists in mathematical modelling. One finds a variety of these used to obtain the numerical results of the book.

InTech Europe
University Campus STeP Ri
Slavka Krautzeka 83/A
51000 Rijeka, Croatia
Phone: +385 (51) 770 447
Fax: +385 (51) 686 166
www.intechopen.com

InTech China
Unit 405, Office Block, Hotel Equatorial Shanghai
No.65, Yan An Road (West), Shanghai, 200040, China
中国上海市延安西路65号上海国际贵都大饭店办公楼405单元
Phone: +86-21-62489820
Fax: +86-21-62489821

IntechOpen